Experimental observations of blast wave formation driven by high-intensity laser interactions with underdense plasma

P M Nilson, S P D Mangles, L Willingale, M C Kaluza, A G R Thomas, M Tatarakis, Z Najmudin, R G Evans[a)], A E Dangor, K Krushelnick

Plasma Physics Group, The Blackett Laboratory, Imperial College London, Prince Consort Road, London, SW7 2BW, UK

R J Clarke, K L Lancaster

Central Laser Facility, CCLRC Rutherford Appleton Laboratory, Chilton, Didcot, Oxon., OX11 0QX, UK

S Karsch, J Schreiber

Max-Planck-Institut für Quantenoptik, Hans-Kopfermann-Straße 1, D-85748 Garching, Germany

[a)] also at AWE plc, Aldermaston, Reading RG7 4PR, UK

Main contact email address: *philip.nilson@imperial.ac.uk*

Introduction

The dynamics of strong blast waves[1)] have been studied extensively in various geometries[2)], principally due to their role in the formation and evolution of astrophysical phenomena[3)]. Laboratory studies of laser-driven blast waves have accessed both the early and late stages of blast wave formation by careful choice of target composition, laser energy, pulse duration, and focused intensity.

Early studies used low-intensity, 100's ps pulse duration laser pulses to heat high-Z gases by inverse bremsstrahlung absorption. Short pulse (ps or fs duration) lasers with moderate intensities (below 10^{17} Wcm^{-2}) have been demonstrated to be an ideal driver for blast wave studies by decoupling the plasma heating phase from the subsequent heat transport and hydrodynamic expansion.

A novel medium for such studies are gases of atomic clusters[4)]. High-temperature plasmas (> 1 keV) can be produced on rapid timescales by virtue of their high-absorption characteristics. Incorporating such targets with short pulse duration laser drivers has enabled the study of non-local electron transport, thermal electron heat wave propagation, and late stage hydrodynamic blast wave formation. Radiative blast waves have similarly been created in high-Z atomic clusters, enabling the study of radiative precursor formation and the radiative properties of the post-shock material.

Most recently, studies have concentrated on the study of blast front instabilities[5)]. The importance of such instabilities depends upon the rate of radiative cooling and heating, the presence of magnetic fields, and the finite thickness of the accelerating or decelerating blast front.

Despite the low absorption characteristics of gases (< 1 %), the Vulcan Petawatt facility offers a novel capability for studying energy absorption, heat transport and hydrodynamic expansion in underdense plasmas by delivering *100's J* in a sub-ps laser pulse (> 10^{20} Wcm^{-2}), achieving an extreme-relativistic intensity regime. In this report, we present optical probing measurements of the initial stages of cylindrically symmetric blast wave formation in helium gas driven by the Vulcan Petawatt Laser. Two important properties are observed; firstly, the front is observed to reduce in thickness over time and, secondly, the front exhibits instability after 200 ps following the termination of the laser pulse.

Experiment

The experiment was performed using the Vulcan Petawatt laser at the Rutherford Appleton Laboratory. A schematic of the experimental layout is given in Figure 1.

The laser delivered pulses of 200 J in 650 fs at a wavelength of 1.054 μm (Nd:glass). The laser was focused onto the edge of a supersonic gas jet target (2 mm nozzle diameter) using an f/3 off-axis parabolic mirror to a vacuum focal spot of 6-7 μm full width at half maximum, with a peak irradiance of $3\text{-}5x10^{20}$ Wcm^{-2}. Helium was used as the target gas. The backing pressure could be varied to give plasma electron densities of up to $5x10^{19}$ cm^{-3}. Analysis of the wavelength-shifted laser light scattered by the Raman forward scattering instability provided a simultaneous measurement of the plasma electron density during the interaction.

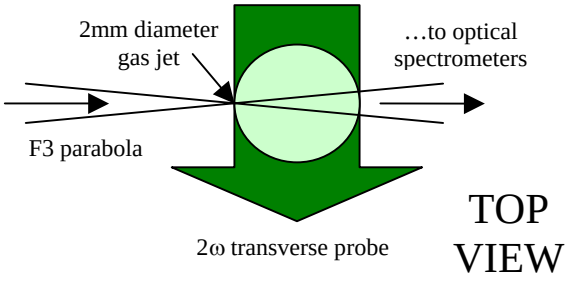

Figure 1. The experimental layout.

The interaction was diagnosed with a temporally independent probe beam in a direction orthogonal to the main interaction. The probe beam was derived from the compressed main beam, providing high temporal resolution, and frequency doubled to 0.527 μm in a KDP (potassium dihydrogen phosphate) crystal. The plasma evolution and blast front structure was monitored by re-imaging the probe beam with 10x magnification and approximately 5 μm resolution.

Results

The plasma evolution was tracked in time to t_0+225 ps. We define t_0 to be the time that the main pulse arrives at the focal plane, marked B in Figure 2 a). The inherent prepulse ensures that the main pulse will interact with a low-temperature, low density plasma.

Figure 2 a) is a shadowgram taken at t_0+10ps. The laser has created a cylindrical channel over 350 μm in length prior to defocusing. At this stage, a cylindrically symmetric, smooth, radially propagating front has formed. The front is 70 μm in radius and 400 μm in length, expanding with a radial velocity of $7x10^{8}$ cms^{-1}.

The laser is observed to filament as it defocuses into a cone of 9^0 half-angle. The filaments extend to the rear of the gas jet. The darkest regions of the filamentary structures indicate high-electron-density gradients where the probe beam has been refracted out of the acceptance angle of the optical system. Ionization tracks are evident at large angles to the rear of the gas jet. These are due to large-angle side-scattering instabilities.

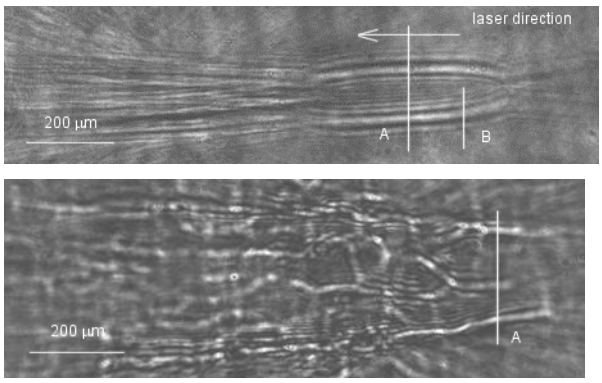

Figure 2. a) Shadowgrams taken at t_0+10ps (above) and **b)** t_0+225ps (below).

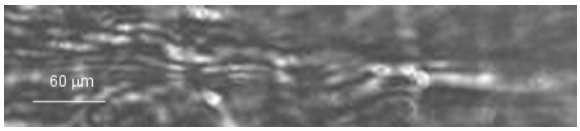

Figure 3. A shadowgram taken at t_0+225ps highlighting the shock front instability.

Figure 2 b) is a shadowgram taken at t_0+225ps. The blast front has been driven into the ambient plasma. Instability has developed on the expanding front. Importantly, Figure 3 demonstrates how this instability has developed without the front fragmenting or breaking-up. Rather, the front maintains an approximately uniform thickness, while the instability has a wavelength and amplitude on the scale of the front thickness itself.

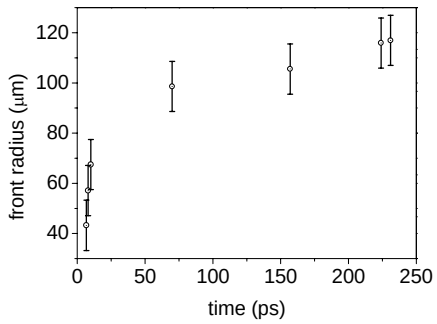

Figure 4. A plot of the temporal variation in blast front radius.

Over a series of shots, the front trajectory was tracked in time by varying the delay of the probe beam with respect to the interaction beam. Figures 4 and 5 show how the blast front radius and thickness vary in time, respectively, along the radial position marked A. The blast front is observed to reduce in thickness from approximately 52 μm to 30 μm between t_0+10ps and t_0+225ps.

Following an initial stage of rapid expansion, the front velocity reduces from $7x10^8 cms^{-1}$ to $1x10^7 cms^{-1}$. The data in Figure 4 are fitted to the expression $R = \beta t^{\alpha}$, where R is the blast front radius. The initial stage of expansion gives α = 1.06 with maximum standard deviation 0.03. During the late stage of expansion, α = 0.18 with maximum standard deviation 0.03.

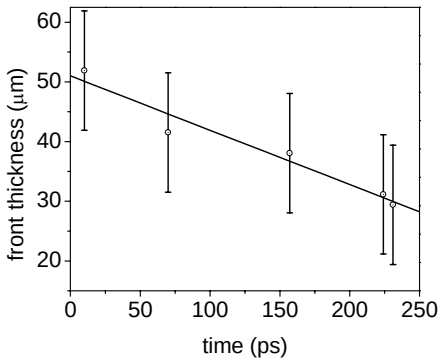

Figure 5. A plot of the temporal variation in blast front thickness.

PIC Simulations

We have undertaken a series of 2D3V particle-in-cell simulations using the code OSIRIS to study the first few picoseconds of plasma evolution. For the simulations presented below, a stationary box was used to observe the plasma evolution following the passage of a laser pulse with a_0 = 15.

The density profile of the fully ionized He plasma was modeled with a 0.1mm ramp to a density of $0.01n_{cr}$, maintained over 0.5mm. The linearly polarized laser beam had a Gaussian profile of 0.65ps duration. The beam was focused to the top of the density ramp, corresponding to a power of 0.4PW. The computational grid has longitudinal (x) and transverse (y) dimensions of 587μm and 168μm respectively.

Figure 6 shows the evolution of plasma parameters along a cross-section taken at the centre of the computational grid. Presented are profiles of n_e, n_i and E2 (the electric field component in the transverse x2 direction) as a function of x2. Only one side of the expanding plasma is given, where x2=500 corresponds to the centre of the laser-generated plasma channel. Note that the scale varies on each plot.

After 0.48ps, the electrons have responded to the laser ponderomotive force. They have been expelled from the axial region, setting up an electric field. The ions initially remain stationary by virtue of their greater inertia.

By 0.8ps, the ions have had imparted upon them a significant impulse and have accelerated to the position of the electron front.

An electric field exists across the combined electron and ion front, caused by the more mobile electrons propagating slightly ahead of the ion front. By 1.2ps, the electron-ion front is propagating at $\approx 10^8 cms^{-1}$ into the upstream ambient gas. We see evidence for a multi-group ion flux; the ions with greater momentum begin to propagate ahead of the main front, presenting a steep density gradient to the ambient gas. A sufficient population of electrons is tied to the forward propagating front, thereby maintaining quasi-neutrality. The lower energy ions are left behind, forming the channel boundary.

In time, the forward propagating front exhibits dispersive behaviour. An electric field develops across the main front due to charge separation. The electric field is zero at the peak of the front, developing a positive field ahead of the density perturbation and a negative field to its rear, respectively. Electrons and ions start to lag the main front and form the emergent backfill of the previously formed cavity.

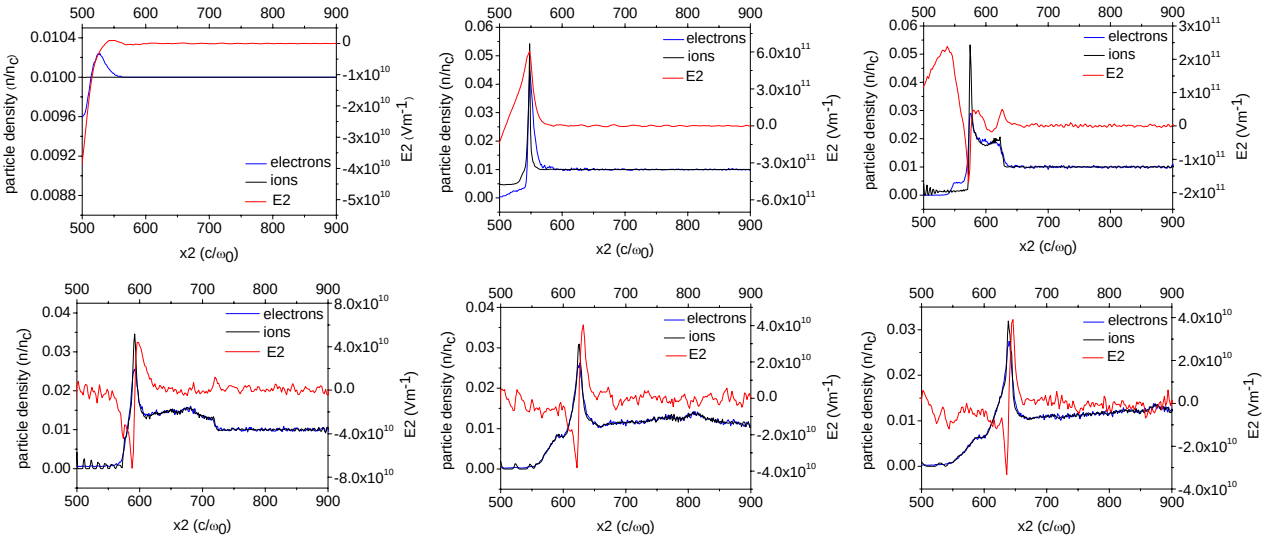

Figure 6. OSIRIS code results for different time steps (0.48 ps, 0.80 ps, 1.20 ps, 1.60 ps, 2.00 ps, 2.80 ps) showing the evolution of electron density, ion density, and the magnitude of the radial electric field. Note the scales vary on each graph.

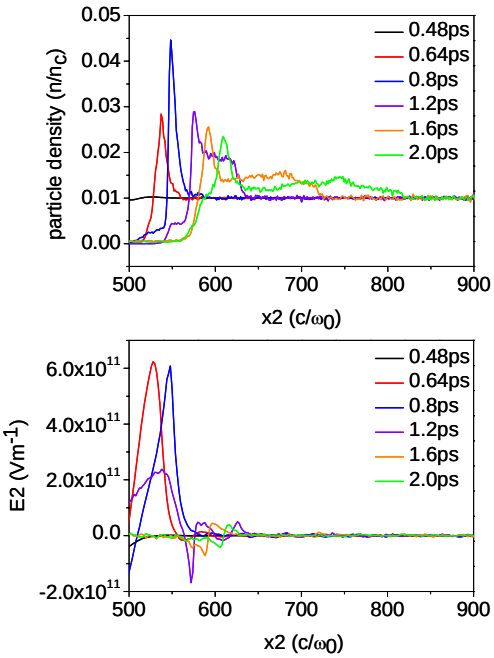

Figure 7. OSIRIS code results for different time steps showing the evolution of electron density (above) and the magnitude of the radial electric field (below).

Over the duration of the simulation the electric field across the front reduces in accordance with energy dissipation and the loss of electrons and ions to the quasi-neutral, forward propagating front, and the quasi-neutral plasma that lags the principal front. This is demonstrated more clearly in Figure 7 where the electric field, E2, and electron density are plotted on the same axis scales. These observations are in qualitative agreement with the previous work of Krushelnick *et al.*[6] and Sarkisov *et al.*[7] at lower intensities.

Discussion

In this Report, optical probing measurements have been presented of the underdense helium plasma response following the passage of a sub-ps laser pulse at intensities of greater than 10^{20} Wcm^{-2}. Interesting features include the reduction in front thickness in time and the onset of instabilities without the front breaking-up or fragmenting. This is different to the case of a hydrodynamic front that increases in thickness as it snow ploughs into the ambient medium, expected to form on longer timescales than are discussed here. The underlying cause of this behaviour is currently under study, and likely to be caused by the affect of relativistic self-focusing on energy-coupling to hot electrons and the resulting multi-group flux of ions generated by the Coulomb explosion mechanism, highlighted by the OSIRIS simulations.

The environment and shock front created here are very different to those recently reported at lower intensities[4] and presents the opportunity to study different classes of blast front and their associated instabilities. Not least, this creates an environment in which to study the transition from weakly collisional to collision dominated behaviour, prior to the classic Sedov-Taylor limit.

Acknowledgements

The authors acknowledge the assistance of the staff of the Central Laser Facility, RAL. We gratefully acknowledge the OSIRIS Consortium, which consists of UCLA / IST (Portugal) / USC for the use of OSIRIS.

References

1. J Von Neumann, 'The point source solution,' National Defense Research Committee, Division B Report AM-9, 1941; G Taylor, 'The formation of blast wave by a very intense explosion,' British Report RC-210, 1941; G Taylor, Proc. R. Soc. A 201, 159 (1950; 201, 175 (1950)); L Sedov, Prokl. Mat. Mekh., 10, 241 (1946); Y Zeldovich, 'Motion of a gas under the action of an impulsive pressure (load),' Akust. Zh. 2, 28-38 (1956); Y Zeldovich and Y Raizer, Physics of Shock Waves and High-Temperature Phenomena (Academic, London, 1966)
2. M Dunne *et al.*, PRL 72, 7 (1994);T Clark and H Milchberg, PRL 78, 12 (1997); J Grun *et al.*, PRL 66, 2738 (1991); T Ditmire *et al.,* PRL 80, 4 (1998)
3. R Chevalier, Ann. Rev. Astron. Astrophys. 15, 175 (1977)
4. M J Edwards *et al.*, PRL 87, 8 (2001); A Moore *et al.*, Phys. Plasmas 12, 052707 (2005)
5. E T Vishniac, ApJ 428, 186 (1994); E T Vishniac, ApJ 274, 152 (1983)
6. K Krushelnick *et al.*, PRL 83, 4 (1999)
7. G S Sarkisov *et al.*, PRE 59, 6 (1999)